Article

Thickness Mediated Morphology Evolution in Sub-10-nm Metal Film Deposition: Implications for Nondestructive Testing

Feng Wang, Yuequn Fu, Senbo Xiao, Bjørn Helge Skallerud, Siqi Liu, Sihai Luo, Helge Kristiansen, Jianying He,* and Zhiliang Zhang*
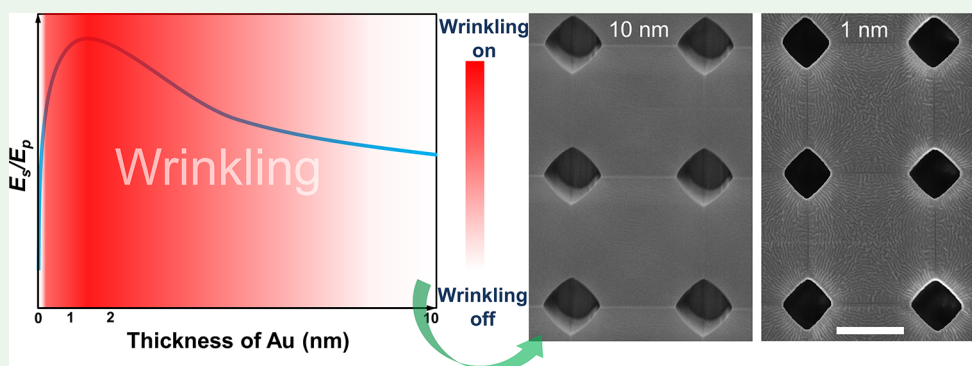
Cite This: ACS Appl. Nano Mater. 2023, 6, 11491–11499

Read Online

ACCESS | Metrics & More | Article Recommendations | Supporting Information

ABSTRACT: Thickness in sub-10-nm metal film deposition is a seldom explored parameter that can influence not only the film mechanical properties but also the surface functional characteristics. In this study, we designed bilayer systems comprising Au on a poly(dimethylsiloxane) (PDMS) substrate to reveal a unique thickness-mediated surface morphology evaluation phenomenon. Our results show that, within a specific range of elastic modulus of the selected PDMS substrate, surface wrinkling starts when the deposited theoretical Au thickness is around 0.2 nm, reaches a maximum deformation at thickness 1−2 nm, and disappears when the thickness is equal to or larger than 8 nm. The thickness-mediated wrinkling on and off suggest that film thickness can strongly impact the patterns observed on soft elastomers. This finding indicates that what we observed may not be the intrinsic surface properties but rather thickness-controlled wrinkling. Using 2 nm Au deposition as a highly sensitive nondestructive testing method, a potential application for identifying surface defects on solid surfaces is proposed.

KEYWORDS: ultrathin metal film, thickness-dependent modulus, elastic modulus, wrinkles, nondestructive testing

INTRODUCTION

With the advances of nanotechnology, ultrathin (<10 nm) metal films have become increasingly important for a wide range of applications including photovoltaic cells,[1,2] optoelectronic devices,[3,4] plasmon-enhanced spectroscopy,[5,6] optical biosensing,[7,8] and transparent conductors.[9−11] For instance, the state-of-the-art transparent conductors rely critically on the indium tin oxide (ITO) films.[4,12] However, the utilization of ITO as the transparent electrode suffers from challenges such as high cost,[13−15] intrinsic brittleness,[16,17] and high refractive index.[18] The ultrathin metal film with tailored conductivity, mechanical robustness, and high optical transparency can serve as a promising candidate for ITO-free organic optoelectronic devices.[4,19] Numerous investigations have been carried out focusing on the adhesion, morphology, and electrical and optical performances of ultrathin metal film.[1,4,20,21] The film thickness in ultrathin metal film deposition, which influences the resulting mechanical properties as well as surface characteristics, has rarely been studied.

For ultrathin films, the surface-to-bulk ratio is much higher, and therefore their mechanical properties are distinct from those of bulk materials.[22−24] Although some theoretical models have been derived for estimating the thickness dependence of elastic modulus in ultrathin metal films, experimental demonstration of the evolution of elastic modulus with film thickness is still challenging.[23,24] First, conventional mechanical tests cannot be directly applied to ultrathin metal films. Moreover, the nanoindentation method that is widely used for measuring the mechanical properties of metal films is not very useful in testing the ultrathin films, because the influences from the substrates are remarkable.[25] Due to the lack of under-
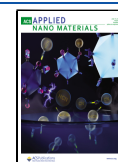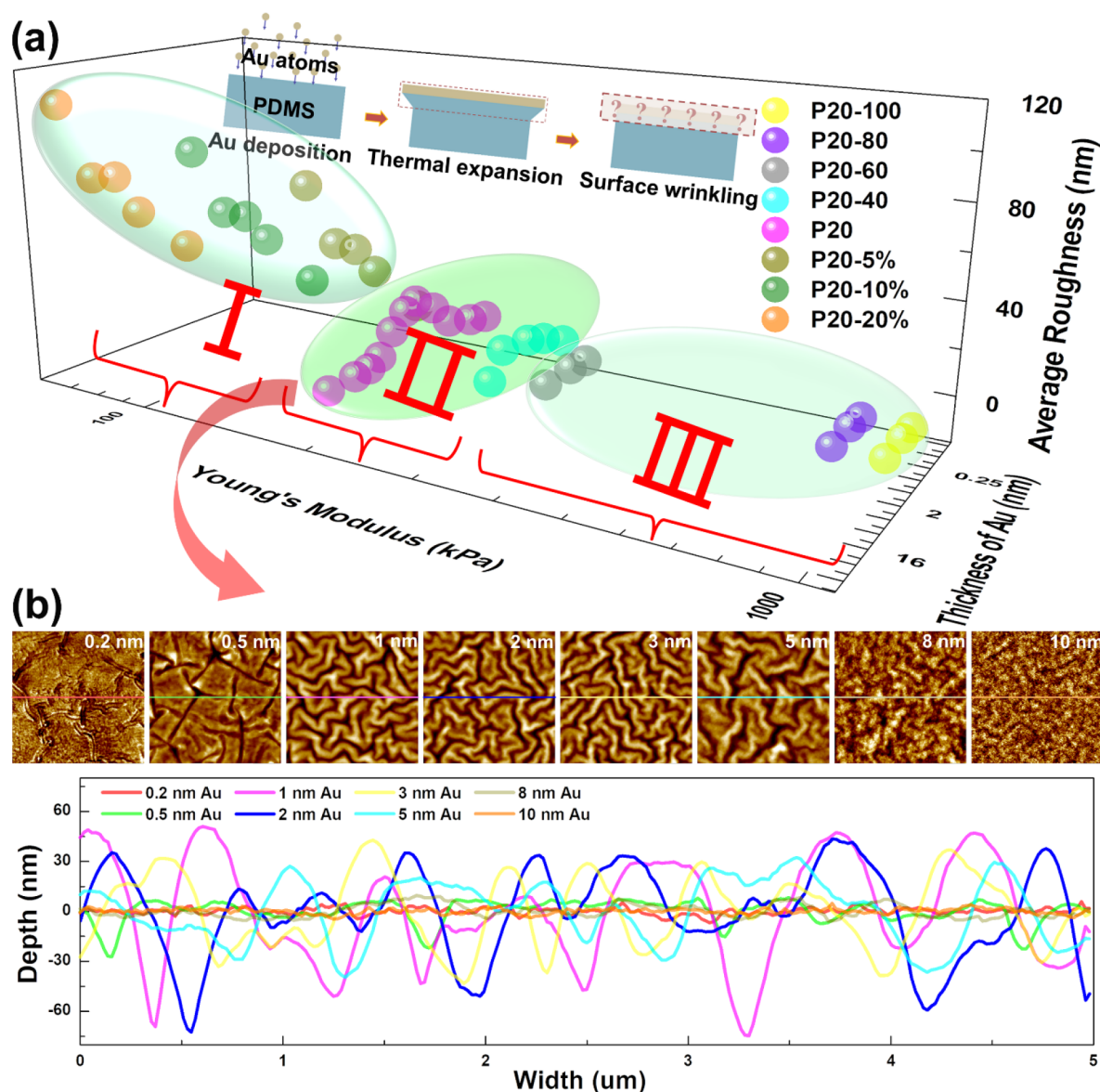
Figure 1. Substrate elastic modulus and film-thickness-mediated surface wrinkling. (a) An inserted schematic diagram shows the process of fabricating surface wrinkles. The 3D plot shows the effects of Young's modulus of PDMS and Au thickness on the surface roughness. Three distinctive regimes of PDMS Young's modulus are identified: Regime I with low modulus where surface wrinkles always occur; Regime II with moderate modulus where surface wrinkling is controlled by the film thickness; Regime III with high modulus where no wrinkles appear. The sample that is cured at room temperature is named P20. Samples that are treated in 40, 60, 80, and 100 °C are named P20−40, P20−60, P20−80, and P20−100, respectively. Samples that are diluted with 5 wt %, 10 wt %, and 20 wt % diluters are named P20−5%, P20−10%, and P20−20%, respectively. (b) The detailed wrinkle evolution on PDMS with Young's modulus of 203 kPa. The plot shows the depth profiles along the midsection lines of the AFM images. The size of the AFM images is 5×5 μm.

standing of the relationship between film thickness and elastic modulus in ultrathin metal films, ultrathin-film thickness has seldom been correlated to surface mechanical responses nor acted as a tool for surface mechanical property control.

In this work, in the case of ultrathin Au film deposition on polydimethylsiloxane (PDMS), we find that film thickness is an unexpected parameter that can be used to modulate the surface morphology by switching on and off surface wrinkling. Theoretical analyses are carried out to correlate this wrinkling on and off phenomena with the evolution of elastic modulus in an ultrathin Au film. Atomistic modeling and molecular dynamics simulation are also employed to investigate the elastic modulus of ultrathin Au films. The experimental and simulation results agree with each other and reveal the

evolution tracks of wrinkling in the ultrathin Au films. The thickness-mediated wrinkling evolution indicates that the film thickness can significantly impact the outcome of the experimental characterization of soft polymer surfaces. We also show that this thickness-dependent variation of the sub-10-nm film can work as a highly sensitive detector in multiple practical applications.

■ RESULTS AND DISCUSSIONS

Switching Surface Wrinkling on and off by Controlling Film Thickness. It is known that wrinkles appear on the surface when the compressive stress in a bilayer system due to property mismatch reaches critical buckling stress (σ_{crit}).[26,27] Metal deposition on the soft polymer is frequently used to
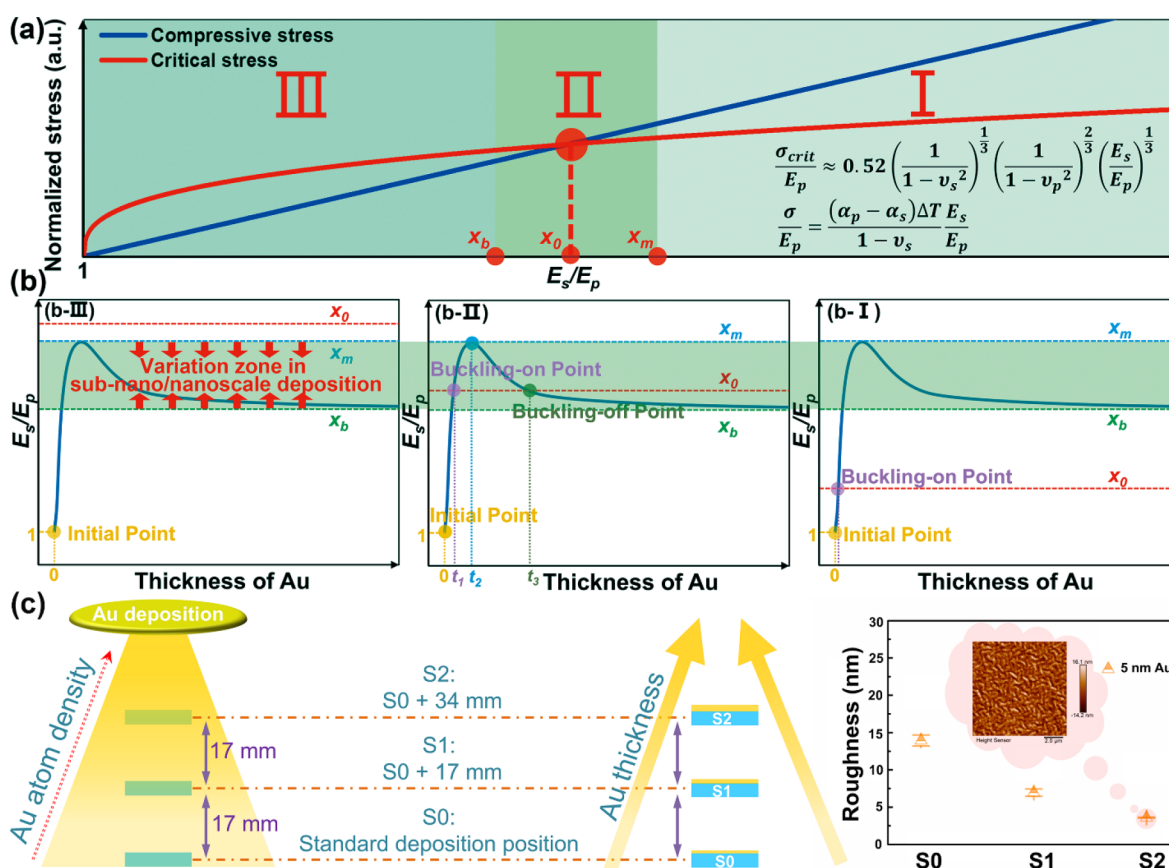
Figure 2. The mechanism behind film thickness-controlled wrinkling on/off. (a) Illustration of the competition between the surface buckling resistance (critical stress) and buckling driving force (compressive stress) in the top surface layer as a function of E_s/E_p. (b) The modulus variation zone with associated scenarios (b-I)−(b-III) depicts the three different regimes I−III shown in Figure 1a. A "buckling-on" region between thicknesses t_1 and t_3 is clarified for regime II. (c) The method that is used for verifying the wrinkling-on/-off phenomenon is caused by the film thickness change.

create surface wrinkles.[26,28−30] To describe the wrinkling caused by thermal contraction after metal deposition, eqs 1 and 2 can be used to estimate the critical stress σ_{crit} for wrinkle formation and the wavelength (λ) of the formed wrinkles[26]

$$\sigma_{crit} \approx 0.52 \left(\frac{E_s}{(1 - v_s^2)} \right)^{1/3} \left(\frac{E_p}{(1 - v_p^2)} \right)^{2/3} \quad (1)$$

$$\lambda \approx 4.36t \left(\frac{E_s(1 - v_p^2)}{E_p(1 - v_s^2)} \right)^{1/3} \quad (2)$$

where E is Young's modulus, ν is Poisson's ratio, and t is the metal film thickness and subscripts s and p refer to the stiff surface layer and the soft elastomer substrate, respectively. Equation 1 shows that the buckling stress and wrinkle formation are independent of the film thickness. Equation 2 indicates that the wavelength of the wrinkle scales linearly with film thickness.

The finding in this work starts with a demonstration of the dependence of surface wrinkling on the PDMS elastic modulus after Au deposition. Wrinkling shall occur when the compressive stress generated in the film has reached the critical value (eq 1). It is evident that increasing the elastic modulus of the substrate increases the threshold for wrinkling. We monitor the wrinkling of Au film by varying Young's modulus of PDMS in a range of 65−1055 kPa (the elasticity of

PDMS and the Au thickness are carefully controlled; see Supplementary Sections1−2). Three distinctive regimes of the PDMS elastic modulus are identified, as exhibited in Figure 1a. In regime I with an elastic modulus lower than 190 kPa, surface wrinkling always occurs. In regime III with an elastic modulus higher than 352 kPa, no surface wrinkles appear, and surface roughness remains unchanged. The selective appearance of surface wrinkles in these two regimes is a good example of using substrate modulus as a known degree of freedom to modulate buckling response (Supplementary Section 3). Surprisingly, in addition to regimes I and III, there is an unexpected regime II with a moderate elastic modulus, which provides a new degree of freedom, namely, the deposited metal thickness, for modulating the surface structures in particular to enable switching-on and -off surface wrinkling.

Samples located in regime II with an elastic modulus of 203 kPa are scrutinized to elaborate on how the surface morphology evolves with film thickness, as shown in Figure 1b. The surface sample (P20 in Figure 1b) before the deposition is smooth from our previous study.[31] The surface turns rough after Au is deposited, reaching the largest surface deformation with Au thickness around 1−2 nm (Figure 1b). Unexpectedly, the subsequent increase in Au thickness reduces the surface roughness and the surface wrinkling is switched off after 8 nm Au is deposited. Initially, when the Au thickness is below 1 nm (i.e., 0.2 and 0.5 nm), the deposited Au is composed of particle clusters. The compression stress
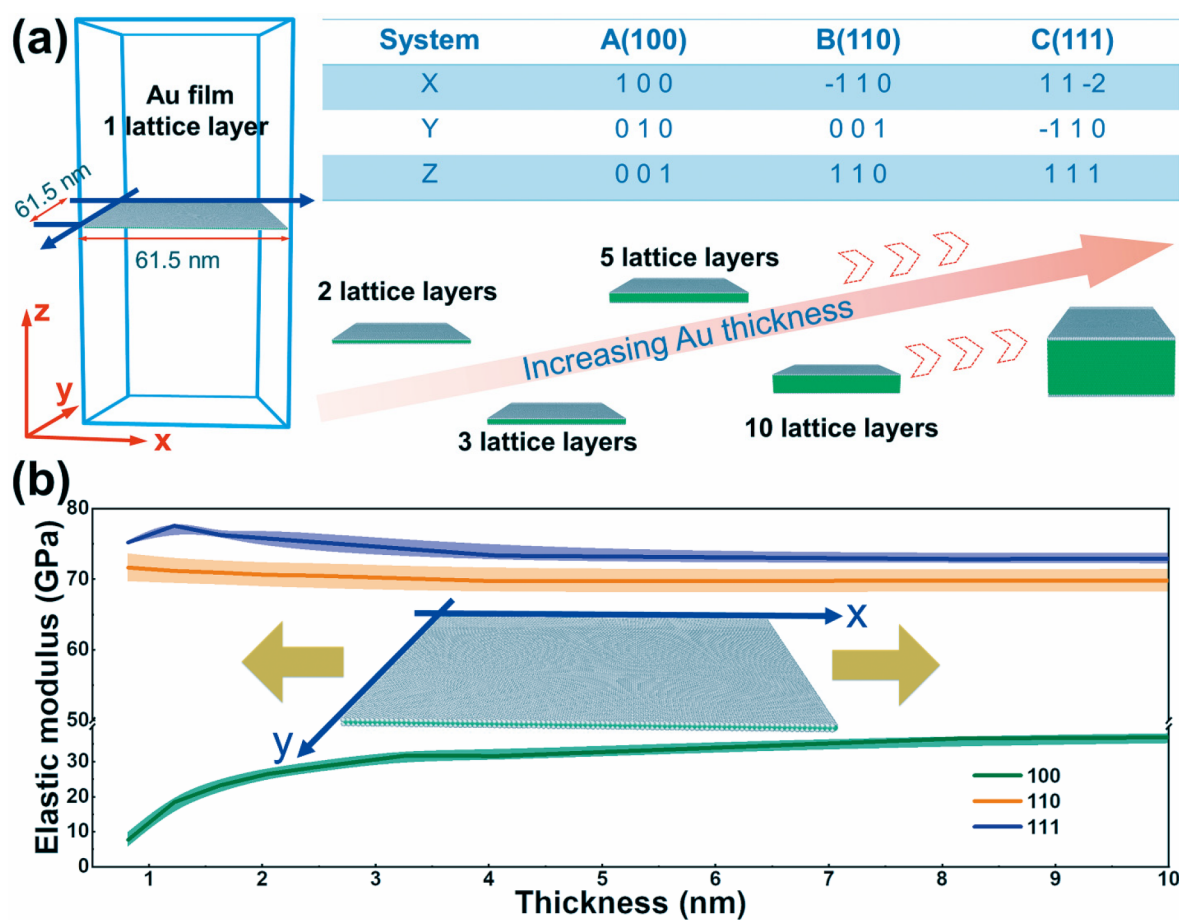
Figure 3. The relationship between Au thickness and elastic modulus through atomistic modeling and molecular dynamics simulation. (a) Representative thin film with a periodic simulation box. Three Au structures with various lattice orientations (100), (110), and (111) are systematically investigated and compared. The thicknesses of the Au films range from 2 to 320 lattice units. (b) The elastic modulus of the ultrathin Au films is plotted as a function of the film thickness. The inset indicates the uniaxial loading direction of the tension tests in the simulations. The color areas adjacent to the three solid curves indicate the standard deviations of the results.

generated in the system is more concentrated in the surroundings of the clusters. Inhomogeneous folds and wrinkles emerged at the regions with concentrated stress 32. The homogeneous film is formed after 1 nm Au is deposited, and then the uniform biaxial compression leads to labyrinth-like wrinkles.[26] According to eq 2 as well as the experiences from other reports, wrinkles keep evolving accompanied by an increase in the wavelength and depth with an increase in the film thickness.[26,32,33] Highly unexpected, however, here upon further deposition of Au, when the film is thicker than 8 nm, wrinkles are switched off and surface smoothness is recovered. This finding indicates that there exists an unexplored parameter affecting surface instability in the ultrathin metal layer deposition.[34]

Thickness-Mediated Wrinkling Revealing Thickness-Dependent Modulus in Ultrathin Film. Variation of surface layer elasticity with the ultrathin film thickness is responsible for the unusual morphology evolution observed in regime II. The equal-biaxial compressive stress (σ) caused by the mismatch of thermal expansion coefficients (α) can be calculated[26]

$$\sigma = \frac{E_s(\alpha_p - \alpha_s)(\Delta T)}{1 - \nu_s} \tag{3}$$

where ΔT is the temperature change in the bilayer system. By using eqs S3 and S4, Supplementary Section 4 and taking ΔT as a constant, we plot the competition between the normalized compressive and critical stress in the surface layer (σ/E_p and σ_{crit}/E_p) as a function of E_s/E_p in Figure 2a. When the two curves cross, a critical buckling point, $E_s/E_p = x_0$, can be identified. It should be noted that for a given PDMS substrate and ΔT, from x_0 we can infer whether the elastic modulus of the surface layer is sufficient to cause buckling. We note that the surface layer in metal deposition begins with a composite of PDMS and Au particle clusters and gradually forms a continuum Au layer. It is reasonable to assume that E_s is a function of the deposition thickness, starting from $E_s/E_p = 1$ and ending at $E_s/E_p = E_{bulk}/E_p$ (E_{bulk} is the bulk elastic modulus of the metal) when the deposited film is sufficiently thick.[23] We further assume that there is a peak value of the elastic modulus of the surface layer, $E_{s, max} > E_{bulk}$. Detailed discussions about the variation of E_s/E_p during deposition are given in Supplementary Sections 5−6. The existence of the unique variation zone can explain the three regimes now reformulated in Figure 2a. For the sake of simplicity, let us define $x_m = E_{s, max}/E_p$, and $x_b = E_{bulk}/E_p$. Figure 2b depicts three alternatives. When E_p is very large and thus $x_0 > x_m$, it indicates that the compressive stress is smaller than the critical buckling stress and surface wrinkling will not be possible (Figure 2b-
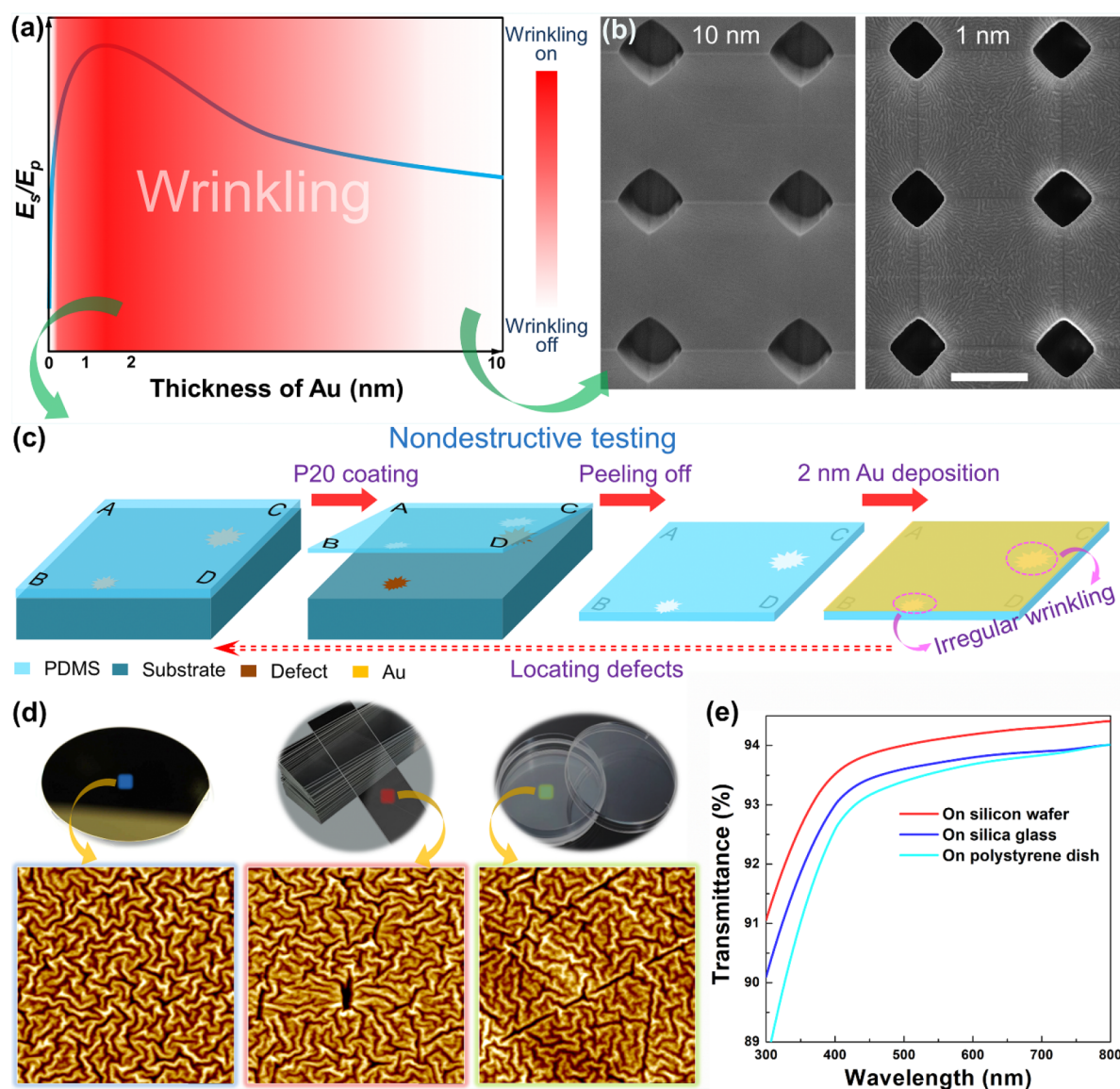
Figure 4. The thickness-dependent wrinkling behaviors and their applications. (a) The curve that correlates the thickness of the ultrathin Au film with wrinkling behaviors. The high likelihood of wrinkles on soft polymer surfaces after depositing different thicknesses of the metal thin film is indicated by the red color with scaling bar. (b) Polymer surface morphology by depositing varied thickness of Au. The scale bar is 10 μm. (c) Enabling the wrinkling of a polymer surface by depositing thin Au and their potential in nondestructive testing. The schematic diagram and examples of the testing process are described using P20 and subsequent 2 nm Au deposition. (d) Three substrates are tested: the silicon wafer, the silica glass, and the polystyrene dish (from left to right). The surface morphologies that can reveal the defects of substrates are given. (e) The transmittances of P20 peeled from various substrates are compared. The size of the AFM images is 10 × 10 μm.

III). For the case with small E_p and $x_0 < x_b$, the compressive stress in the surface layer is so large that it will always cause wrinkling (Figure 2b-I). On the contrary, surface wrinkling will occur at first and then be switched off gradually upon further deposition if the condition $x_b \leq x_0 \leq x_m$ is satisfied (Figure 2b-II). In regime II, surface roughening starts at a film thickness of t_1, attains a maximum amplitude at t_2, and the roughness is switched off at t_3 ($t_3 > t_2 > t_1$). The increment of $\Delta t = t_3 - t_1$ is a useful indicator for controlling the thickness window where the roughness can be switched on. For instance, we obtain that $t_1 = 0.2$ nm, $t_2 = 2$ nm, and $t_3 = 8$ nm for our substrate sample P20. By increasing the elastic modulus of PDMS, taking the P20−40 sample for example, the variation zone of E_s/E_p reduces, and the "switched-on" window becomes narrower ($\Delta t' < \Delta t$, Supplementary Figure S14). Supplementary Figure

S5 shows that the P20−40 surface starts wrinkling at 0.2 nm deposition and returns to smooth after the deposition of 5 nm Au, which agrees well with the discussion above. Further increasing the elastic modulus of PDMS will suppress the surface roughness. In parallel, by decreasing Young's modulus of PDMS, the variation range of E_s/E_p expands and the "switching-on" window turns wider ($\Delta t'' > \Delta t$, Supplementary Figure S14). Further decreasing the elastic modulus of PDMS will move toward regime I where surface wrinkling and roughness are always observed.

To further verify that the wrinkling-on-/-off phenomenon is attributed to the film thickness instead of the deposition time, surfaces are deposited with the method shown in Figure 2c. In this case, the deposition thickness can be tuned within the same deposition time by modulating their distance to the Au

target. By elevating the PDMS from a standard deposition position (S0) to S1 and S2 shown in Figure 2c, thicker Au can be deposited on the surfaces. After a targeted 5 nm (the thickness at S0) deposition, we compared the surface appearances from different locations. As shown by the curve in Figure.2c, we can see that the surfaces after deposition gradually turn smooth from S0 to S2. The surface roughness evolution trend indicates that the elastic modulus of the Au film gradually decreases with increasing thickness after 5 nm.

Relationship between Atomistic Au Thickness and Elastic Modulus. Atomistic modeling and molecular dynamics simulation are used to elucidate the dependence of the elastic modulus of ultrathin Au films on their thickness. As shown in Figure 3a, perfect Au films with face-centered-cubic (FCC) lattice structures are constructed for this purpose. All the films have an area of 20×20 cubic lattice units and are periodic in the plain directions (x- and y-axis of the simulation box shown in Figure 3a). The thicknesses of Au films range from 2 to 320 lattice units, corresponding to 0.816, 1.224, 1.632, 2.04, 2.448, 3.264, 4.08, 8.16, 16.32, 32.64, 65.28, and 130.56 nm. For each thickness, three films with lattice orientations of (100), (110), and (111) along the x-axis direction of the simulation box are built for uniaxial tension tests. The length of the box in the z-axis is at least five times the thickness of the ultrathin films to avoid atomistic interactions across the periodic box boundary, as shown by the empty spaces in the simulations box in Figure 3a. During the tensile tests, stress and strain in each film are collected for quantifying the elastic modulus (E_{Au}). The relationship between calculated E_{Au} and film thickness (0–10 nm) is shown here, and the others are given in Supplementary Section 7) in three systems are shown in Figure 3b. Additionally, a bulk Au crystal consisting of periodic $20 \times 20 \times 20$ cubic lattice units is used for comparison, the elastic modulus of which obtained by the same simulation procedure is denoted as E_{bulk}. The calculated E_{bulk} values for lattice orientations of (100), (110), and (111) are 38.0, 69.1, and 72.0 GPa, respectively. Obviously, for the (100) orientation, the E_{Au} gradually increases with increasing film thickness. The films with the (110) orientation along the x-axis show decreased trend in modulus with increasing Au thickness. Interestingly, the elastic modulus of Au with lattice orientations of (111) along the x-axis increases at first and then decreases with further increases in film thickness. With large film thickness (>60 nm as indicated in Supplementary Figure S16), the bulk modulus of each orientation is generally approached and maintained.

In a thin metal film deposition on an amorphous substrate, the growth of grains with (111) texture is generally favored over the growth of grains with other orientations in FCC materials such as gold.[35] This can be attributed to that (111) planes have minimum surface energy for free surfaces and interfaces without reacting with the underneath substrates.[36] Experimental results also confirmed that 25 nm Au film growth on SiO_2 had a strong (111) peak which indicated the growth of grains at lattice orientations of (111) in ultrathin films.[37] Therefore, the elastic modulus evolution in the lattice orientation of (111) shows the representative thickness-dependence in the ultrathin Au film. It is fair to say that the simulation results suggest E_{Au} of ultrathin Au film increases at first and then decreases with the increase of Au thickness. With the results shown in Figure 3b, there exists an $E_{Au,\ max}$ at a thickness of 1.224 nm in an ultrathin Au film. The result agrees

with the observation in the above experiments that $1 \sim 2$ nm Au films have the highest modulus.

Notably, thickness-dependent modulus evolution can be reproduced using other metals. In extra experiments of depositing ultrathin Pt/Pd on P20, the thickness-dependent wrinkling, -on/-off, is also discovered. The surface of P20 starts wrinkling at 0.2 nm deposition and returns to smooth after 3.5 nm Pt/Pd is deposited (Supplementary Figure S17). Therefore, the predictable wrinkling behaviors by metal deposition can be a universal method to control the surface morphology of ultrathin metal films.

Utilizing Thickness-Dependent Modulus of Ultrathin Au Film for Multiple Applications. With the above analyses, in the case of ultrathin Au depositing on PDMS, we know that wrinkling is expected to occur with 1−2 nm Au deposition and is less possible to happen with Au thickness approaching 10 nm (Figure 4a). The control of surface smoothness and roughness on demand is of substantial interest,[38,39] in particular in revealing the true surface properties.

On the one hand, maintaining the smoothness of a polymer surface after metal deposition is essential for subsequent surface detection. Thicker Au with a lower elastic modulus is suggested to avoid surface wrinkling. Scanning electron microscopy (SEM) is commonly used to evaluate surface morphology, in which metal coatings in the range of 1−10 nm are needed to detect nonconductive materials. The influence of metal deposition on the surface morphology has often been ignored. Figure.4b shows two SEM images for P20−40 with arrays of pores after 1 and 10 nm Au deposition, respectively. The surface with 10 nm Au deposition reveals a smooth surface. However, the surface with 1 nm Au deposition develops unwanted wrinkles. The surface wrinkles can lead to misinterpretation of the surface structures of PDMS. In this regard, to reveal the true surface morphology of soft materials through SEM, the coating thickness of metal should be carefully chosen to avoid misinterpretation of the wrinkles generated by sputtering deposition, or better deposition guidelines should be introduced.

On the other hand, enabling the deformation of a polymer surface after metal deposition can act as a useful technology for nondestructive testing. Au with the highest elastic modulus around 1−2 nm is suggested to enhance surface wrinkling. The scenario of utilizing the wrinkling behaviors of 2 nm Au deposition for nondestructive testing is proposed in Figure 4c. Solid surfaces (such as glasses and plastics) are generally not perfectly smooth, containing invisible defects/inhomogeneities. Direct observation of surface defects remains a challenge. By coating P20 onto a solid substrate, the defect on the solid surface can influence the assembly of the polymer at the contact area in the curing process. As a result, the defect will create an imprint on the contacted polymer surface after PDMS solidification. The imprint is invisible; however, it can affect the subsequent wrinkling behaviors. Irregular wrinkles were found on P20 surfaces at the imprint area after 2 nm Au deposition. Therefore, one can locate the defect on the solid with information provided by surface wrinkles. We show the demonstrations of three solid surfaces, the silicon wafer surface, the silica glass surface, and the polystyrene dish surface, which are tested by the proposed procedure. Obviously, after deposition, homogeneous wrinkles are observed on P20 peeled off from the silicon wafer, while irregular wrinkling regions are observed on P20 peeled off from

silica glass and polystyrene dish (Figure 4d). The results indicate that the surface of the silicon wafer is smoother than the surfaces of silica glass and a polystyrene dish. The irregular wrinkles resulted from the imprints on P20. Consequently, the corresponding defects/inhomogeneities on the silica glass or polystyrene dish surfaces can be detected. Notably, the above process avoids direct measurement of the solid surfaces, which minimizes the possible damage of the surface structures in contactable testing. Moreover, the PDMS can be coated onto and peeled off surfaces easily even with surface curvatures, hence providing an effective strategy for detecting solids with complex shapes. We also show that the transparencies of P20 coatings that are peeled off from various substrates are different from each other (Figure 4e). Generally, high transmittance is desired for PDMS films in various optical applications.[40−42] To date, the effects of substrates on PDMS transparency have not been realized. With the curves in Figure 4c, we can conclude that the smoothness of the substrates greatly determines the transparency of fabricated PDMS films. PDMS fabricated on silicon wafers shows higher transmittance than that on silica glass or polystyrene dish surfaces. Previous discussions have pointed out that surface defects will influence the assembly of polymer chains during PDMS curing at the contacted area. Subsequently, inhomogeneous regions are formed at the side in contact with the substrate with defects. Therefore, to obtain PDMS with high transparency, perfect surfaces like silicon wafers are suggested to be used as substrates.

CONCLUSIONS

In this work, through depositing sub-10-nm Au on a PDMS substrate with appropriate elastic modulus, a thickness-dependent wrinkling phenomenon is reported. The wrinkling behaviors on the surfaces after deposition are strongly correlated with the film elastic modulus. By increasing the thickness of Au, the surface follows a pattern of wrinkling on, reaching maximum deformation, and wrinkling off after a specific thickness is achieved. Supported by abundant experimental results and theoretical analyses, we conclude that the Young's modulus of the Au film is closely related to film thickness. Molecular dynamics simulation reveals the same modulus dependence on the Au film thickness. We also show that a precise understanding of the modulus evolution and the corresponding wrinkling on surfaces can potentially lead to various novel applications. On the one hand, well-controlled Au deposition thickness should be taken into consideration in experimental characterization to avoid surface wrinkling for the purpose of revealing the true surface characteristics. On the other hand, enabling surface wrinkling with 2 nm Au deposition can provide a powerful tool for nondestructive testing. We believe that the visualized evidence of the thickness-dependent modulus in ultrathin Au films not only can improve the understanding of the mechanical properties of ultrathin metal films but also can promote the usage of ultrathin metal films in practice.

MATERIALS AND METHODS

Materials Synthesis. Polydimethylsiloxane (PDMS) with different elasticity is synthesized as soft substrates in the bilayer system. PDMS prepolymer (Sylgard 184, Dow Corning) and curing agent are mixed in a weight ratio of 10:1. The final mixtures are degassed in a vacuum chamber and then placed at room temperature (20 °C) for 51 h to obtain cured PDMS, namely P20. To achieve PDMS with higher Young's modulus, samples after curing for 50 h are transferred into an oven with various temperatures and held for 1 h. Samples treated at 40, 60, 80, and 100 °C are named as P20−40, P20−60, P20−80, and P20−100, respectively. To achieve PDMS with lower Young's modulus, diluent (DOWSIL OS-20, Dow Corning) is introduced into the mixture of PDMS prepolymer and curing agent. Diluent with mass contents of 5 wt%, 10 wt%, 20 wt%, and 40 wt% to the PDMS prepolymer is added into the mixtures and are named P20−5%, P20−10%, P20−20%, and P20−40%, respectively. Diluted samples are cured by the same process of P20. PDMS with holes is fabricated by coating a liquid mixture on the template. The microstructure of the template is shown in Figure S26. The silicon wafers with pillars are silanized with trichloro(1H,1H,2H,2H-perfluorooocty)silane (Sigma-Aldrich) in a vacuum chamber for 8 h before coating. After curing and peeling off PDMS from the silicon wafer, P20−40 with microholes are obtained. In the process of nondestructive testing, silicon wafer, silica glass, and polystyrene dish are first washed with ethanol (Sigma-Aldrich) before P20 coating. The P20 films on the three substrates are fabricated with the same method above. The thickness of all PDMS is controlled at 1.82 ± 0.02 mm.

Metal Deposition. PDMS is cut into the size of 1 cm × 1 cm and put into a vacuum chamber of sputter coater (208 HR B, Cressington) incorporated with MTM-20 High-Resolution Thickness Controller for sputtering deposition; the resolution of the controller exceeds 0.1 nm. The metal target is ∼ 60 mm above the sample surfaces. The metal targets of Au and Pt/Pd were used in this work. The argon gas pressure and sputtering current are fixed at 0.02 mbar and 20 mA. The tooling factor of the MTM-20 controller used is 1.8. The density for Au deposition is 19.30 g/cm^3, and the density for Pt/Pd deposition is 19.52 g/cm^3. The sputtering rate is 0.15 nm/s. To investigate the thickness-dependent modulus of the ultrathin metal film, the top surfaces of PDMS without contact with substrates are used for Au deposition to ensure their smoothness. On the contrary, the bottom surfaces of PDMS that are in contact with substrates are taken to Au deposition for nondestructive testing.

Characterization. The mechanical properties of PDMS are measured through quasi-static nanoindentation tests in a Tri-boIndenter 950 (Hysitron, Inc.) by using a cylindrical diamond flat punch with 53.70 ± 0.06 μm diameter. Thicknesses of the PDMS are measured by a digimatic micrometer (Mitutoyo, ID-C112GB). The surface topographies and three-dimensional information are recorded by Atomic Force Microscopy (AFM, Dimension Icon, Bruker) using a ScanAsyst in air mode. The average roughness, average depth, and wavelength are calculated from AFM images using the methods described in the previous study.[31] The morphologies of silicon wafers with pillars and PDMS with holes are characterized by a field-emission scanning electron microscope (FEI APREO SEM).

Simulation. The Large-scale Atomic/Molecular Massively Parallel Simulator (LAMMPS) package is chosen to perform all the molecular dynamics simulations.[43] The well-calibrated Au embedded atom method (EAM) potential[44] is chosen for describing the interactions between Au atoms, which is confirmed to yield accurate mechanical properties of the Au.[45] The time step is set as 1 fs in all simulations. The NVT ensemble (constant number of particles, constant volume, and constant temperature) is applied in the simulations. Specifically, a Nosé-Hoover thermostat with a damping time constant of 100 is used to control the temperature (298 K). The uniaxial stress loading is performed by extending the corresponding box length with a constant strain rate of 1.0×10^{10} s^{-1}. The uniaxial tensile loading on each ultrathin Au film stopped at a strain value of 0.01.

ASSOCIATED CONTENT

Ⓢ Supporting Information

The Supporting Information is available free of charge at https://pubs.acs.org/doi/10.1021/acsanm.3c01533.

Additional experimental details and descriptions of the materials, substrates, characterization, and methods (PDF)

■ AUTHOR INFORMATION

Corresponding Authors

Jianying He − *Department of Structural Engineering, Norwegian University of Science and Technology (NTNU), Trondheim 7491, Norway;* orcid.org/0000-0001-8485-7893; Email: jianying.he@ntnu.no

Zhiliang Zhang − *Department of Structural Engineering, Norwegian University of Science and Technology (NTNU), Trondheim 7491, Norway;* orcid.org/0000-0002-9557-3455; Email: zhiliang.zhang@ntnu.no

Authors

Feng Wang − *Department of Structural Engineering, Norwegian University of Science and Technology (NTNU), Trondheim 7491, Norway; Foshan (Southern China) Institute for New Materials, Foshan 528231, China; Shenzhen Adventure Tech Co., Ltd., Shenzhen 518000, China;* orcid.org/0000-0002-6112-2824

Yuequn Fu − *Department of Structural Engineering, Norwegian University of Science and Technology (NTNU), Trondheim 7491, Norway*

Senbo Xiao − *Department of Structural Engineering, Norwegian University of Science and Technology (NTNU), Trondheim 7491, Norway*

Bjørn Helge Skallerud − *Department of Structural Engineering, Norwegian University of Science and Technology (NTNU), Trondheim 7491, Norway*

Siqi Liu − *Department of Structural Engineering, Norwegian University of Science and Technology (NTNU), Trondheim 7491, Norway*

Sihai Luo − *Department of Chemistry, Norwegian University of Science and Technology (NTNU), Trondheim 7491, Norway;* orcid.org/0000-0001-5614-9734

Helge Kristiansen − *Department of Structural Engineering, Norwegian University of Science and Technology (NTNU), Trondheim 7491, Norway*

Complete contact information is available at:
https://pubs.acs.org/10.1021/acsanm.3c01533

Notes

The authors declare no competing financial interest.

■ REFERENCES

(1) Zou, J.; Li, C. Z.; Chang, C. Y.; Yip, H. L.; Jen, A. K. Y. Interfacial engineering of ultrathin metal film transparent electrode for flexible organic photovoltaic cells. *Adv. Mater.* **2014**, *26* (22), 3618−3623.

(2) Massiot, I.; Cattoni, A.; Collin, S. Progress and prospects for ultrathin solar cells. *Nature Energy* **2020**, *5* (12), 959−972.

(3) Yun, J. Ultrathin metal films for transparent electrodes of flexible optoelectronic devices. *Advanced Functional Materials* **2017**, *27* (18), 1606641.

(4) Bi, Y. G.; Liu, Y. F.; Zhang, X. L.; Yin, D.; Wang, W. Q.; Feng, J.; Sun, H. B. Ultrathin Metal Films as the Transparent Electrode in ITO-Free Organic Optoelectronic Devices. *Advanced Optical Materials* **2019**, *7* (6), 1800778.

(5) Gray, S. K. Surface plasmon-enhanced spectroscopy and photochemistry. *Plasmonics* **2007**, *2* (3), 143−146.

(6) Maniyara, R. A.; Rodrigo, D.; Yu, R.; Canet-Ferrer, J.; Ghosh, D. S.; Yongsunthon, R.; Baker, D. E.; Rezikyan, A.; Garcia de Abajo, F. J.; Pruneri, V. Tunable plasmons in ultrathin metal films. *Nature Photonics* **2019**, *13* (5), 328−333.

(7) Abutoama, M.; Abdulhalim, I. Self-referenced biosensor based on thin dielectric grating combined with thin metal film. *Optics express* **2015**, *23* (22), 28667−28682.

(8) Singh, P. SPR biosensors: historical perspectives and current challenges. *Sensors and actuators B: Chemical* **2016**, *229*, 110−130.

(9) Zhang, C.; Ji, C.; Park, Y. B.; Guo, L. J. Thin-Metal-Film-Based Transparent Conductors: Material Preparation, Optical Design, and Device Applications. *Advanced Optical Materials* **2021**, *9* (3), 2001298.

(10) Ji, C.; Liu, D.; Zhang, C.; Guo, L. J. Ultrathin-metal-film-based transparent electrodes with relative transmittance surpassing 100%. *Nature communications* **2020**, *11* (1), 1−8.

(11) Luo, S.; Lian, E.; He, J.; deMello, J. C. Flexible Transparent Electrodes Formed from Template-Patterned Thin-Film Silver. *Adv. Mater.* **2023**, 2300058.

(12) Betz, U.; Kharrazi Olsson, M.; Marthy, J.; Escola, M.F.; Atamny, F. Thin films engineering of indium tin oxide: large area flat panel displays application. *Surf. Coat. Technol.* **2006**, *200* (20−21), 5751−5759.

(13) Dolley, T. *Mineral Commodity Summaries 2014*; U.S. Geological Survey, 2014; pp 138−139.

(14) Ye, S.; Rathmell, A. R.; Chen, Z.; Stewart, I. E.; Wiley, B. J. Metal nanowire networks: the next generation of transparent conductors. *Advanced materials* **2014**, *26* (39), 6670−6687.

(15) Azzopardi, B.; Emmott, C. J.; Urbina, A.; Krebs, F. C.; Mutale, J.; Nelson, J. Economic assessment of solar electricity production from organic-based photovoltaic modules in a domestic environment. *Energy & Environmental Science* **2011**, *4* (10), 3741−3753.

(16) Inganäs, O. Avoiding indium. *Nature Photonics* **2011**, *5* (4), 201−202.

(17) Hecht, D. S.; Hu, L.; Irvin, G. Emerging transparent electrodes based on thin films of carbon nanotubes, graphene, and metallic nanostructures. *Advanced materials* **2011**, *23* (13), 1482−1513.

(18) Cao, W.; Li, J.; Chen, H.; Xue, J. Transparent electrodes for organic optoelectronic devices: a review. *Journal of Photonics for energy* **2014**, *4* (1), 040990.

(19) O'Connor, B.; Haughn, C.; An, K.-H.; Pipe, K. P.; Shtein, M. Transparent and conductive electrodes based on unpatterned, thin metal films. *Appl. Phys. Lett.* **2008**, *93* (22), 433.

(20) Yakubovsky, D. I.; Stebunov, Y. V.; Kirtaev, R. V.; Ermolaev, G. A.; Mironov, M. S.; Novikov, S. M.; Arsenin, A. V.; Volkov, V. S. Ultrathin and ultrasmooth gold films on monolayer MoS2. *Advanced Materials Interfaces* **2019**, *6* (13), 1900196.

(21) Stec, H. M.; Williams, R. J.; Jones, T. S.; Hatton, R. A. Ultrathin Transparent Au Electrodes for Organic Photovoltaics Fabricated Using a Mixed Mono-Molecular Nucleation Layer. *Advanced Functional Materials* **2011**, *21* (9), 1709−1716.

(22) Nix, W. D. Mechanical properties of thin films. *Metallurgical transactions A* **1989**, *20* (11), 2217.

(23) Zhang, T.-Y.; Wang, Z.-J.; Chan, W.-K. Eigenstress model for surface stress of solids. *Physical Review B* **2010**, *81* (19), 195427.

(24) Fedorchenko, A. I.; Wang, A.-B.; Cheng, H. H. Thickness dependence of nanofilm elastic modulus. *Appl. Phys. Lett.* **2009**, *94* (15), 152111.

(25) Saha, R.; Nix, W. D. Effects of the substrate on the determination of thin film mechanical properties by nanoindentation. *Acta materialia* **2002**, *50* (1), 23−38.

(26) Bowden, N.; Brittain, S.; Evans, A. G.; Hutchinson, J. W.; Whitesides, G. M. Spontaneous formation of ordered structures in thin films of metals supported on an elastomeric polymer. *Nature* **1998**, *393* (6681), 146.

(27) Allen, H. G., *Analysis and Design of Structural Sandwich Panels*; The Commonwealth and International Library: Structures and Solid Body Mechanics Division; Elsevier: 2013.

(28) Das, A.; Banerji, A.; Mukherjee, R. Programming feature size in the thermal wrinkling of metal polymer bilayer by modulating substrate viscoelasticity. *ACS applied materials & interfaces* **2017**, *9* (27), 23255−23262.

(29) Chen, S.; Hu, K.; Yan, S.; Ma, T.; Deng, X.; Zhang, W.; Yin, J.; Jiang, X. Dynamic metal patterns of wrinkles based on photosensitive layers. *Science Bulletin* **2022**, *67* (21), 2186−2195.

(30) Zeng, S.; Yang, Z.; Hou, Z.; Park, C.; Jones, M. D.; Ding, H.; Shen, K.; Smith, A. T.; Jin, H. X.; Wang, B.; et al. Dynamic multifunctional devices enabled by ultrathin metal nanocoatings with optical/photothermal and morphological versatility. *Proceedings of the National Academy of Sciences* **2022**, *119* (4), e2118991119.

(31) Wang, F.; Xiao, S.; Luo, S.; Fu, Y.; Skallerud, B. r. H.; Kristiansen, H.; Cui, M.; Zhong, C.; Liu, S.; Zhuo, Y.; He, J.; Zhang, Z. Surface Wrinkling with Memory for Programming Adhesion and Wettability. *ACS Applied Nano Materials* **2023**, *6* (6), 4097−4104.

(32) Yu, S.; Sun, Y.; Li, S.; Ni, Y. Harnessing fold-to-wrinkle transition and hierarchical wrinkling on soft material surfaces by regulating substrate stiffness and sputtering flux. *Soft Matter* **2018**, *14* (32), 6745−6755.

(33) Shao, Y.; Brook, M. A. Structured metal films on silicone elastomers. *Journal of Materials Chemistry* **2010**, *20* (39), 8548−8556.

(34) Osmani, B.; Deyhle, H.; Töpper, T.; Pfohl, T.; Müller, B. Gold Layers on Elastomers near the Critical Stress Regime. *Advanced Materials Technologies* **2017**, *2* (10), 1700105.

(35) Thompson, C. V.; Carel, R. Stress and grain growth in thin films. *Journal of the Mechanics and Physics of Solids* **1996**, *44* (5), 657−673.

(36) Winterbottom, W.; Gjostein, N. Determination of the anisotropy of surface energy of metals—II: Experimental γ-plot of gold. *Acta Metallurgica* **1966**, *14* (9), 1041−1052.

(37) Wong, C. C.; Smith, H. I.; Thompson, C. Surface-energy-driven secondary grain growth in thin Au films. *Applied physics letters* **1986**, *48* (5), 335−337.

(38) Wang, Y.; Liu, Q.; Zhang, J.; Hong, T.; Sun, W.; Tang, L.; Arnold, E.; Suo, Z.; Hong, W.; Ren, Z.; Guo, C. F. Giant Poisson's Effect for Wrinkle-Free Stretchable Transparent Electrodes. *Adv. Mater.* **2019**, *31*, 1902955.

(39) Wang, T.; Yang, Y.; Fu, C.; Liu, F.; Wang, K.; Xu, F. Wrinkling and smoothing of a soft shell. *Journal of the Mechanics and Physics of Solids* **2020**, *134*, 103738.

(40) Qi, D.; Zhang, K.; Tian, G.; Jiang, B.; Huang, Y. Stretchable electronics based on PDMS substrates. *Adv. Mater.* **2021**, *33* (6), 2003155.

(41) Martin, S.; Bhushan, B. Transparent, wear-resistant, super-hydrophobic and superoleophobic poly (dimethylsiloxane)(PDMS) surfaces. *Journal of colloid and interface science* **2017**, *488*, 118−126.

(42) Guan, F.; Song, Z.; Xin, F.; Wang, H.; Yu, D.; Li, G.; Liu, W. Preparation of hydrophobic transparent paper via using polydimethylsiloxane as transparent agent. *Journal of Bioresources and Bioproducts* **2020**, *5* (1), 37−43.

(43) Plimpton, S.; Hendrickson, B. In *Parallel Molecular Dynamics Algorithms for Simulation of Molecular Systems*; ACS Symposium Series; American Chemical Society: 1995; pp 114.

(44) Foiles, S.; Baskes, M.; Daw, M. S. Embedded-atom-method functions for the fcc metals Cu, Ag, Au, Ni, Pd, Pt, and their alloys. *Physical review B* **1986**, *33* (12), 7983.

(45) Gan, Y.; Chen, J. Molecular dynamics study of size, temperature and strain rate effects on mechanical properties of gold nanofilms. *Appl. Phys. A: Mater. Sci. Process.* **2009**, *95* (2), 357−362.